

# Stretching-enhanced triboelectric nanogenerator for efficient wind energy scavenging and ultrasensitive strain sensing

Xue Zhao<sup>a,b,1</sup>, Ding Zhang<sup>a,d,1</sup>, Suwen Xu<sup>a</sup>, Weiqi Qian<sup>a,d</sup>, Wei Han<sup>b,\*\*</sup>, Zhong Lin Wang<sup>a,c,\*\*\*</sup>, Ya Yang<sup>a,d,e,\*</sup>

<sup>a</sup> CAS Center for Excellence in Nanoscience, Beijing Key Laboratory of Micro-nano Energy and Sensor, Beijing Institute of Nanoenergy and Nanosystems, Chinese Academy of Sciences, Beijing, 100083, PR China

<sup>b</sup> Key Laboratory of Physics and Technology for Advanced Batteries (Ministry of Education), Jilin University, Changchun, 130012, PR China

<sup>c</sup> School of Material Science and Engineering, Georgia Institute of Technology, Atlanta, GA, 30332-0245, USA

<sup>d</sup> School of Nanoscience and Technology, University of Chinese Academy of Sciences, Beijing, 100049, PR China

<sup>e</sup> Center on Nanoenergy Research, School of Physical Science and Technology, Guangxi University, Nanning, 530004, PR China

## ARTICLE INFO

### Keywords:

Triboelectric nanogenerator  
Wind energy  
Stretching enhancement  
Strain sensing

## ABSTRACT

The development of intelligent electronic devices increasingly facilitates the configuration of smart city. However, the heavy using of Li-ion batteries can cause high cost and a series of environmental pollution owing to frequent charging induced by their limited electric capacity. Here, we report a stretching-enhanced triboelectric nanogenerator for efficient wind energy scavenging and ultrasensitive strain sensing based on stretchable composites. The output voltage and current signals can be dramatically increased by 220% and 380% by applying a 70% stretched strain as compared with that under the condition of 0% strain, which is associated with the stretched strain-induced increase of contact area. Moreover, the corresponding output power can be increased by 680% due to the stretched strain of 70%, while the impedance can be decreased by 58.3%. A high strain sensitivity of 1.75 ln(V) or 0.97 ln(Hz) under the stretched strains ranged from 0% to 45% can be obtained as a self-powered strain sensor.

## 1. Introduction

The fast development of smart city is inseparable from various smart electronics that need to consume a large amount of electric energy [1,2]. As the most basic and important power units, Li-ion battery and supercapacitor will lead to high cost and frequent charging owing to the limited electric capacity and further cause a series of environmental pollution [3–5]. As one of most important energy technologies in new era, triboelectric nanogenerator (TENG) have developed rapidly in the past decade due to its advantages of pollution-free, small size, low cost and simple structure, which can efficiently convert mechanical energy into electricity [6–10]. TENGs can not only scavenge wind [11,12], vibration [13,14], wave [15,16] and droplet [17,18] energies from nature,

but also biomechanical energy [8,19,20] including human breathing, heartbeat, and movement energies, etc. On the basis of TENG, the derived hybridized and coupled nanogenerators can simultaneously scavenge mechanical, thermal or solar energies [21–23]. Instead of directly driving electronic devices as power sources [24,25], TENGs have played a key role in e-skin [26,27], human-machine interfaces [28], health monitoring [8,20,29] and self-powered sensing [26,30] etc. It is an ideal solution to scavenge various energies to drive electronic devices, exhibiting the concept of sustainable development for the construction of smart city [1,2].

Wind energy is a common renewable energy and ubiquitous in prosperous city and remote village. Wind-induced TENGs are regarded as one of the most promising energy technologies in the grim context of

\* Corresponding author. CAS Center for Excellence in Nanoscience, Beijing Key Laboratory of Micro-nano Energy and Sensor, Beijing Institute of Nanoenergy and Nanosystems, Chinese Academy of Sciences, Beijing, 100083, PR China.

\*\* Corresponding author.

\*\*\* Corresponding author. CAS Center for Excellence in Nanoscience, Beijing Key Laboratory of Micro-nano Energy and Sensor, Beijing Institute of Nanoenergy and Nanosystems, Chinese Academy of Sciences, Beijing, 100083, PR China.

E-mail addresses: [whan@jlu.edu.cn](mailto:whan@jlu.edu.cn) (W. Han), [zhong.wang@mse.gatech.edu](mailto:zhong.wang@mse.gatech.edu) (Z.L. Wang), [yayang@binn.cas.cn](mailto:yayang@binn.cas.cn) (Y. Yang).

<sup>1</sup> Xue Zhao and Ding Zhang contributed equally to this work.

fossil energy shortage and environmental pollution [2,10–12]. Whereas, wind-induced TENGs are usually rigid and hard, it seems that such TENGs maybe not meet the development needs of flexible and stretchable electronic devices. Flexible TENGs have been reported for power source and self-powered sensor by scavenging biomechanical energy [31–33], however, stretchable wind-induced TENGs as self-powered strain sensors are rarely reported. It is urgent to develop high-performance and stretchable TENGs for scavenging wind energy to realize self-powered strain sensing. Graphene has attracted much attention from researchers in all walks of life since its discovery in 2004 [34], owing to excellent electric and thermal conductivity [35,36]. Stretchable graphene-polymer composites have exhibited remarkable self-powered performance in strain sensing fields due to excellent electric conductivity and stability [37–39]. In addition, the mature preparation technology can acquire controllable graphene film deposition on a stretchable polymer matrix through a precise vacuum filtration process [39–41]. There are many conductive materials as the triboelectric materials or electrodes of flexible TENGs, such as graphite [42] and carbon nanotubes (CNTs) [43], which exhibit satisfactory performance. After a series of preliminary comparisons, the surfaces of fabricated graphite/CNTs-PDMS film show macroscopically rough morphology due to larger graphite sheets, smaller size of CNTs, and short crosslinking time of PDMS precursor. Graphene is a relatively suitable material owing to uniform surface and excellent electrical conductivity of the fabricated graphene-PDMS film, which meet desirable requirements of flexible TENGs.

Here, we report a stretching-enhanced TENG for efficient wind energy scavenging and ultrasensitive strain sensing based on stretchable graphene-PDMS and PTFE-PDMS composites by a vacuum filtration method. The TENG exhibits excellent stretchability and electric property, and the output voltage and current of the TENG can be increased by 220% and 380% from  $\sim 40$  V/1.5  $\mu$ A to  $\sim 128$  V/7.2  $\mu$ A by applying a stretched strain of 70%, respectively, as compared with that under no strains. Moreover, under the stretched strain of 70%, an increase of 680% for the output power and a decrease of 58.3% for the impedance by comparing the data from 0.021 mW/12 M $\Omega$  to 0.164 mW/5 M $\Omega$ , respectively. The enhancement mechanism has been discussed by using a high-speed camera to obtain the vibration information under the different strain conditions. By scavenging wind energy, the TENG can charge a 220  $\mu$ F capacitor to 1 V in 160 s. As a stretchable strain sensor, through measuring output voltage and vibration frequency, it presents a high strain sensitivity of 1.75 ln(V)/% or 0.97 ln(Hz)/% at the strains ranged from 0% to 45%, respectively. This research presents a new method of enhancing the output performances of TENG by stretching the device, which has the potential applications in smart city for driving electronic devices as a power source and self-powered strain sensing by scavenging wind energy.

## 2. Experimental section

**Preparation of graphene-PDMS nanocomposites.** The graphene-PDMS nanocomposite film was prepared through a reported vacuum filtration solution [39,41]. Briefly, 4.2 g of graphene slurry (3.0 w.t% graphene) and 120 mg Cetyl trimethyl ammonium bromide (CTAB) as surfactant were dissolved in 100 mL deionized water forming a homogeneous solution under stirring. Subsequently, 10 mL graphene/CTAB solution was filtrated onto filter membrane (PVDF membrane, pore size: 0.22  $\mu$ m), then washed by deionized water and ethanol. After drying, the filter membrane with graphene on the top side was fixed at the bottom of a homemade acrylic mould, then PDMS precursor solution (mixed PDMS precursor solution and curing agent in a mass ratio of 15:1) was poured into the acrylic mould for crosslinking with graphene. After being degassed in a vacuum chamber, the graphene-PDMS was thermally cured at 80  $^{\circ}$ C for 1 h. Finally, the graphene-PDMS nanocomposite film was carefully peeled off from the acrylic mould. The thickness of the nanocomposite films was controlled by adjusting the amount of PDMS

precursor. Lastly, all specimens were cut into the same size of 40 mm  $\times$  10 mm in following experiments.

**Fabrication of stretchable PTFE-PDMS nanocomposite film.** The preparation process is similar with graphene-PDMS, through vacuum filtration, two filter membrane with PTFE nanoparticles on the top side was obtained. One filter membrane was fixed at the bottom of a homemade acrylic mould, then PDMS precursor solution was poured into the acrylic mould, and another membrane was placed on the top side of PDMS precursor solution. The acrylic mould was at 80  $^{\circ}$ C for crosslinking between PDMS and PTFE. After 1 h, the PTFE-PDMS nanocomposite film was carefully peeled off from the acrylic mould.

**Characterization and Measurements.** The morphologies of graphene-PDMS and PTFE-PDMS nanocomposite were observed by a field-emission scanning electron microscope (SEM, Nova450). The optical photographs of TENG with different stretched strains were observed by an optical microscopy (NIKON, LV100ND). The output voltage and current signals were measured by using a mixed domain oscilloscope (Tektronix, MDO3024) and a low noise current preamplifier (Stanford Research Systems, SR570), respectively. The  $I$ - $V$  curves were performed by a source meter (Keithley, 2611B). The vibration conditions of the TENG at different strains were recorded by a high-speed camera.

## 3. Results and discussion

Fig. 1a exhibits the preparation diagram of the fabrication process of the stretchable graphene-PDMS nanocomposites, including two main processes: (i) precise deposition of graphene on PVDF filter film through a mature vacuum filtration technology; (ii) naturally physical crosslink between graphene and PDMS. Detailed operation procedures are described in Experimental Section. Fig. 1b and c displays the scanning electron microscopy (SEM) images of surface and cross-section of graphene-PDMS nanocomposite film, respectively. The randomly distributed graphene sheets with wrinkled structure are observed on the composite film surface, and the thickness of graphene layer is  $\sim 28$   $\mu$ m, which reveals the formation of graphene layer and the bilayer configuration of graphene-PDMS nanocomposite film. By using a modified and similar preparation process, PTFE nanoparticles were deposited on the top and bottom sides of PDMS method, and the stretchable PTFE-PDMS nanocomposite film was fabricated with sandwich structure. The surface and cross-section SEM images are displayed in Fig. 1d and e, respectively, PTFE nanoparticles uniformly appear on the composite film surface, and the thickness of PTFE layer is about 24  $\mu$ m. The total thickness of graphene-PDMS and PTFE-PDMS films are about 1 and 2 mm, respectively, and all specimens were cut into the same size of 40 mm  $\times$  10 mm in following experiments.

Through the PDMS based graphene and PTFE composites above, a flexible and stretchable TENG was fabricated for scavenging wind energy. Fig. 2a displays the structure diagram, the stretchable TENG consists of two parallel graphene-PDMS nanocomposite films and a flexible PDVF-PDMS film between them. Two sides of each films were fixed by using acrylic plates, and the distance between adjacent films was controllable through changing the thickness of acrylic spacers. Moreover, two Al foils were attached to graphene layers of two graphene-PDMS films as upper and bottom electrodes. Fig. 2b displays the optical image of the fabricated TENG, and the effective dimension of suspended film is 32 mm  $\times$  10 mm. In order to illustrate the stretchability of the TENG and the ability to monitor stretched strains according to resistance variation, the graphene-PDMS film with effective size of 32 mm  $\times$  10 mm was stretched in 0–70% strain range. Fig. 2c and d displays the photographs of the TENG at two strains of 0% and 70%, indicating the excellent stretchability of graphene-PDMS film. Here, the strain is defined as  $\varepsilon = (l - l_0)/l_0 \times 100\%$ , where  $l_0$  and  $l$  are original and stretched length of the film, respectively. The current-voltage ( $I$ - $V$ ) curves of graphene-PDMS film were characterized by stretching the graphene-PDMS film with effective dimension of 32 mm  $\times$  10 mm from 0% to 70% strain, as shown in Fig. 2e. After calculation, the

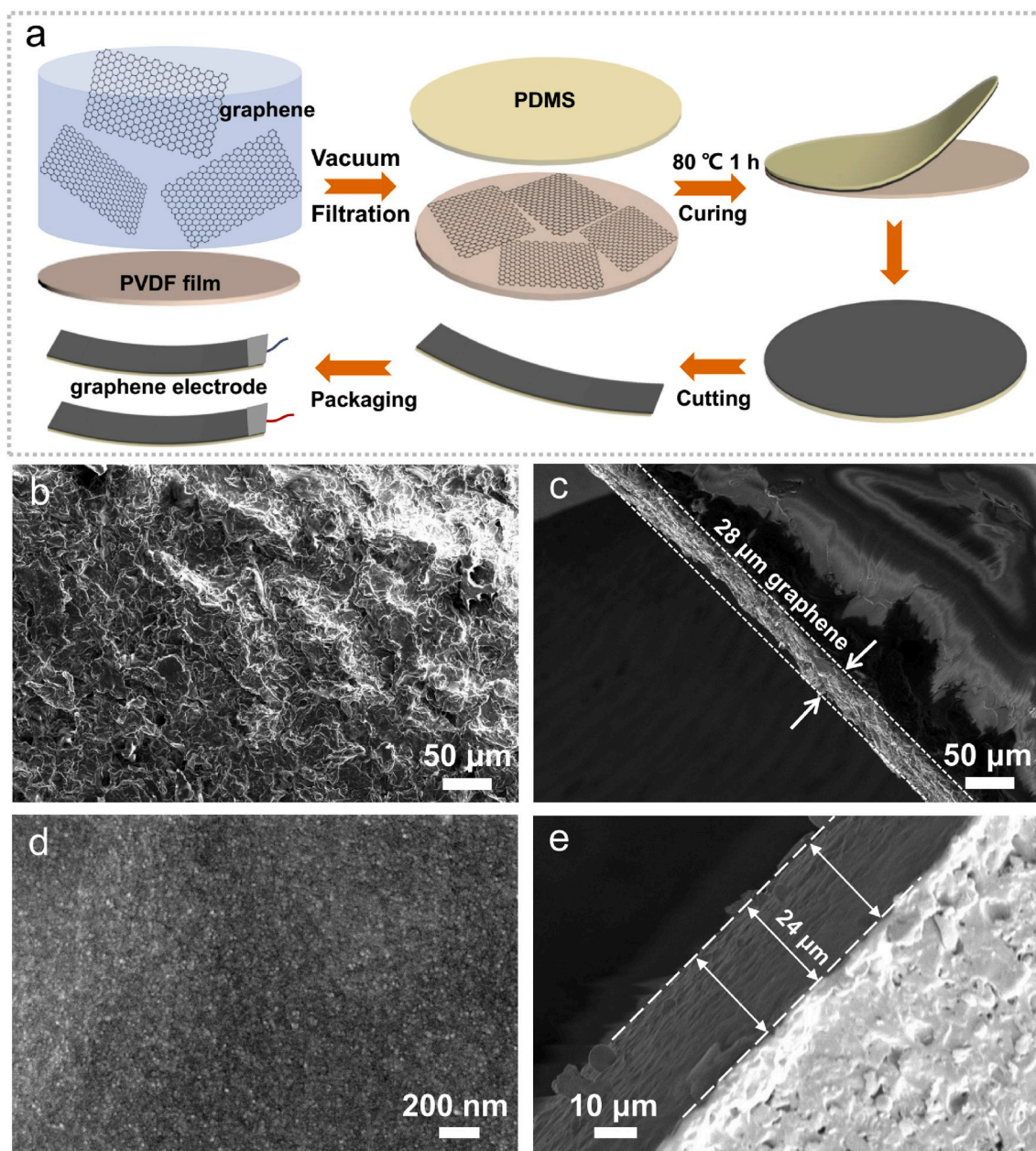


**Fig. 1.** Preparation and characterization of the graphene/PTFE-PDMS composites. (a) Preparation diagram of whole fabrication process of the stretchable graphene-PDMS nanocomposites. (b) SEM image of graphene-PDMS film surface. (c) SEM image of cross-section of graphene-PDMS film. (d) SEM image of surface of PTFE-PDMS film. (e) SEM image of cross-section of PTFE-PDMS film.

corresponding resistance-strain curve shows a monotonously increased tendency of resistance with the strain ranging from 0% to 70%, as exhibited in Fig. 2f, which confirms the feasibility of graphene-PDMS film as a gauge to measure strain  $\epsilon$ . The curve can be linearly fitted into two functions corresponding to the following fitting formulas:

$$\text{when } \epsilon \leq 45\%, R = 19\epsilon + 3.92 \text{ (k}\Omega\text{)} \quad (1)$$

$$\text{and } 45\% < \epsilon \leq 70\%, R = 158\epsilon - 59.96 \text{ (k}\Omega\text{)} \quad (2)$$

The fitting formulas present the same tendency with the theoretical and practical results of previous research reports [44,45]. The larger slope of the fitting formula in  $45\% < \epsilon$  range may result from the slip between graphene sheets on surface of the stretchable composite film [45]. The inset of Fig. 2f displays the variation of gauge factor defined as  $(R - R_0)/(R_0\epsilon)$ , and the gauge factor increases from 3.7 at 5% strain to 16.5 at 70% strain, suggesting the remarkable strain monitoring

performance of the stretchable TENG.

Fig. S1 (Supporting Information) demonstrates the working mechanism of this TENG for harvesting wind-induced vibration energy in this work. Upper and bottom graphene layers periodically contact and separate with the middle PTFE film in turn, owing to triboelectrification and electrostatic induction effects, which will cause opposite charges on graphene and PTFE layers, periodic electron migration between two electrodes. Therefore, the generated electric signals are alternating current (AC) in external circuit. Firstly, to improve output performance of the stretchable TENG, we systematically evaluate the effect of distance between graphene and PTFE layers through changing the thickness of acrylic spacers (0.5, 1.0, 1.5, 2.0, 3.0, 4.0 mm) at different strains ranged from 0% to 80% strains. The corresponding output voltage and output current of the TENG are obtained at the same air flow speed of about 15 m/s. Unless otherwise specified, all air flow speed in follow-up experiments was kept at 15 m/s. As displayed in Figs. S2–S7 (Supporting

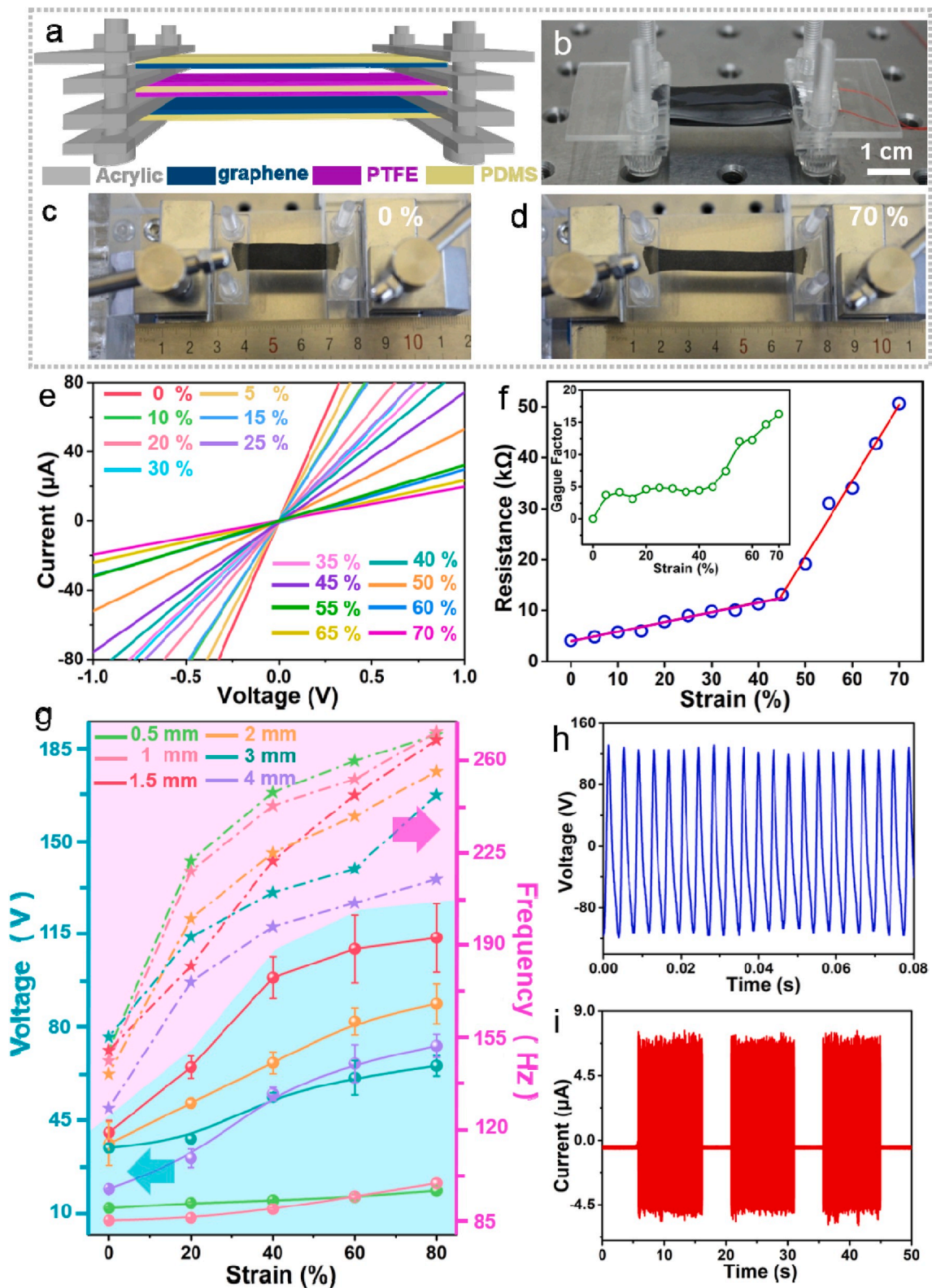


Fig. 2. Design and performance optimization of the stretchable TENG. (a) Schematic diagram of the stretchable TENG. (b) Photograph of the stretchable TENG. (c,d) Photograph of the stretchable TENG at 0% strain (c) and 70% strain (d). (e)  $I$ - $V$  curves of graphene-PDMS film. (f) Resistance-strain curve of the graphene-PDMS. (g) The output voltage and vibration frequency of the TENG with different spacer thickness. (h,i) The output voltage (h) and short-circuit current (i) signals of the stretchable TENG.

Information), and it can be observed that all the output voltage and the output current present an increasing tendency with the increase of stretched strain. Taking the output voltage signals for example, Fig. 2g illustrates the average output voltage and vibration frequency of TENG with different thickness of acrylic spacer at different strains level. For each thickness of acrylic spacer, both the average output voltage and vibration frequency of TENG gradually increase with the increasing stretched strain. When the thickness of acrylic spacer is 0.5 or 1.0 mm, the TENG exhibits the greater vibration frequency but the smaller the output voltage. As seen from Fig. S8 (Supporting Information), it's obvious that the TENG with spacer thickness of 1.5 mm can deliver the greatest average output voltage ranging from 40 to 114 V corresponding to the stretched strain of 0%–80%, so the spacer thickness of all stretchable TENGs was kept at 1.5 mm in the following experiments. Then, the output signals of the TENG at a stretched strain of 70% were researched, and Fig. 2h and i depicts the corresponding output voltage and the output current with a vibration frequency of 268 Hz. The generated voltage and the output current reach up to 128 V and 7.2  $\mu$ A,

respectively, and the small difference of positive and negative electrical signals may be caused by incomplete symmetry of the two graphene-PDMS films.

At present, increasing researchers are committed to improving the output power of TENGs to meet the needs of practical applications [46, 47]. To obtain the largest output power, the output performances of the TENG at different strains were systematically investigated. Fig. 3a and b illustrates the dependence of the output voltage and corresponding power on the external loading resistance at 0% and 70% strain, respectively, in addition, the output performances of the TENG at 20%, 40% and 60% strain were also researched as depicted in Fig. S9 (Supporting Information). We can see that the output voltage of the TENG all monotonically increase with increasing external resistance owing to the Ohmic loss, and the corresponding output power first increase and then decrease gradually. The external loading resistance corresponding to the maximum power is equal to the internal resistance of the TENG. Fig. 3c describes the dependence of internal resistance and maximum power of the TENG on the applied strain, and it's worth noting that the resistance

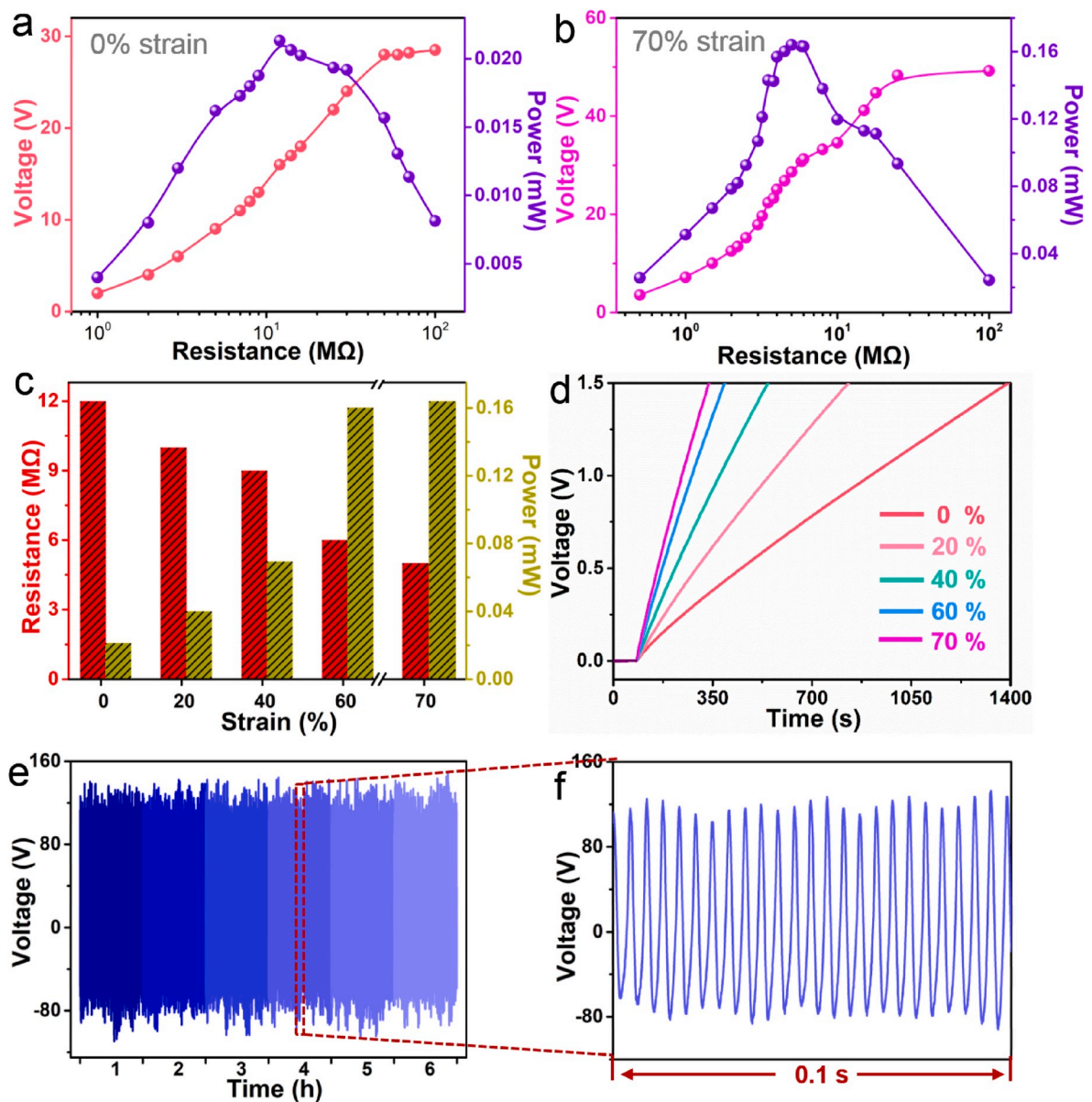


Fig. 3. Electrical output performance and stability of the TENG. (a,b) Dependence of the output voltage and corresponding instantaneous power of the TENG at 0% (a) and 70% strain (b). (c) Dependence of internal resistance and maximum power of the TENG at different strains. (d) Charging curves of a 220  $\mu$ F capacitor by the TENG at different strains. (e,f) Stability of the time-dependent output voltage of the TENG.

of graphene-PDMS composite film presents a growing tendency with the increasing strain in Fig. 2f. Whereas, the internal resistance of TENG gradually decrease from 12 to 5 M $\Omega$  in working process corresponding to the increasing stretched strain from 0% to 70%, which may result from the increase of generated positive/negative charges induced by the increasing contact area between graphene and PTFE layers in vibration process. Compared with the maximum output power of 0.021 mW at the initial condition of 0% strain, by applying stretched strain of 70%, the maximum output power greatly increased by 680% up to 0.164 mW. To explore power supply performance as a power source at different strains, a 220  $\mu$ F capacitor was charged by the wind-induced TENG with a rectifier that can convert the AC signal into DC signal. Fig. 3d displays the charging curves of the capacitor by the TENG at different stretched strain, the greater the strain, the faster the charging. When the TENG was at 70% strain, the capacitor can be charged from 0 to 1.0 V in 160 s far less than that of 0% strain. Fig. 3e shows the output voltage stability of the TENG for harvesting wind energy with the air flow speed of about 15 m/s, where the output voltage curve of 0.1 s was enlarged in Fig. 3f. The TENG exhibit excellent cyclic stability and durability for 6 h more than 500,000 vibration cycles.

To better study the possible relationship between vibration conditions and output signals of the TENG, and in order to further enhance output performance by optimizing structure design and even material selection in the follow-up work, the vibration conditions of the TENG at different strains were recorded by a high-speed camera (Revealer, 2F04). Fig. 4a presents the photographs of the TENG in one vibration cycle at the strain of 0%, and the top and bottom graphene layers periodically contact and separate with PTFE layer in turn. The contact situations of the graphene layer and PTFE layer of the films at different stretched strain (0%, 20%, 40%, 60%, 70%) in vibration process were also recorded, as shown in Fig. 4b and Figs. S10–S14 (Supporting Information). The relative location variation of each film at different stretched strain were counted and summarized in Fig. 4c, and we can see that the displacements of the top and bottom films are relatively larger than that of the middle film. The displacement difference of the top and bottom films illustrates the incomplete symmetry structure of the stretchable TENG, and properly corresponds to the small difference of positive and negative electrical signals in Fig. 2h and i. At the strain of 0%, the TENG is in relatively relaxed state and easy to deform with a large relative displacement, whereas the vibration frequency is smaller

than others. When applying a small stretch-strain, the amplitude of the TENG will be small in vibration process. With the increase of stretched strain, the relative displacement of the top and bottom vibrational films increases gradually, which may be caused by the increased vibration frequency of the films approaching to the inherent frequency of the TENG. The average contact area and corresponding ratio of contact area and the total area of the films were calculated and exhibited in Fig. 4d. Both the contact area and the ratio (contact/total area) gradually increase with an increasing strain, which contributes to the increase of positive/negative charges at interface between graphene and PTFE, and further enhance the voltage and current signals at a macro-view level. In addition, the discussion above can also explain and confirm the research result of Fig. 3c that the internal resistance of TENG decrease gradually with the increase of stretched strain from 0% to 70%.

To investigate the strain sensing property of the TENG, the effect of stretched strain on the output voltage of the TENG was demonstrated by harvesting wind energy. Different strains were applied to the TENG, ranged from 0% to 70% strains. Fig. 5a and Fig. S15 (Supporting Information) show the lateral and vertical view of the TENG at different stretched strain, respectively. According to the vertical view, we can see that the width of graphene-PDMS composite film decreases gradually with a growing strain. Figs. S16–S18 (Supporting Information) describes the output voltage and the output current of the TENG under different strain. As exhibited in Fig. 5b and c, both the output voltage and corresponding vibration frequency present an increasing tendency with the increase of stretched strain. At a stretched strain ranging from 0% to 70%, the corresponding output voltage and vibration frequency monotonically increase from 40 V to 128 V and 150 Hz–268 Hz, respectively. Through natural logarithmic fitting, the linear relationships between the output voltage/vibration frequency and corresponding different strain range are acquired, as shown in Fig. 5d. The slopes of linear fitting curves can be expressed as strain sensitivity of the TENG up to 1.75 and 0.65 ln(V) corresponding to the stretched strain of 0% <  $\epsilon$  < 45% and 50% <  $\epsilon$  < 70%, respectively. By using vibration frequency as a gauge to measure strain, the corresponding strain sensitivity of the TENG is respectively up to 0.97 and 0.4 ln(Hz), which also indicates that the stretchable TENG as a strain sensor can realize self-powered and ultra-sensitive strain sensing by harvesting wind energy.

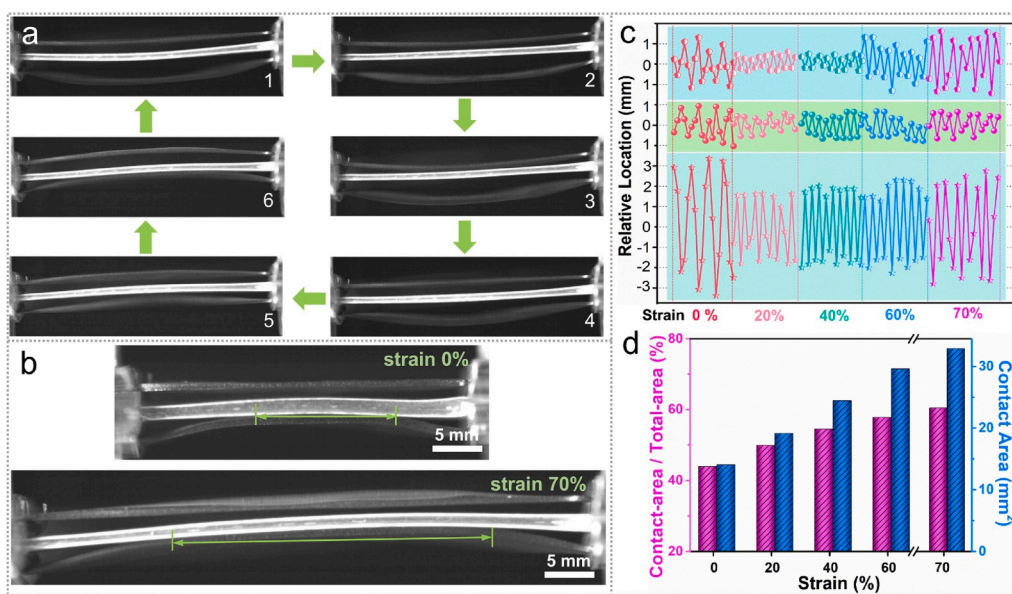


Fig. 4. Contact analysis of vibration films. (a) Photographs of vibration process of the TENG in one cycle. (b) Contact conditions of graphene and PTFE layer of the TENG at 0% and 70% strain. (c) Relative location of the top and bottom graphene-PDMS films and PTFE-PDMS film in vibration process. (d) Dependence of contact area between graphene and PTFE layer on the applied strain.

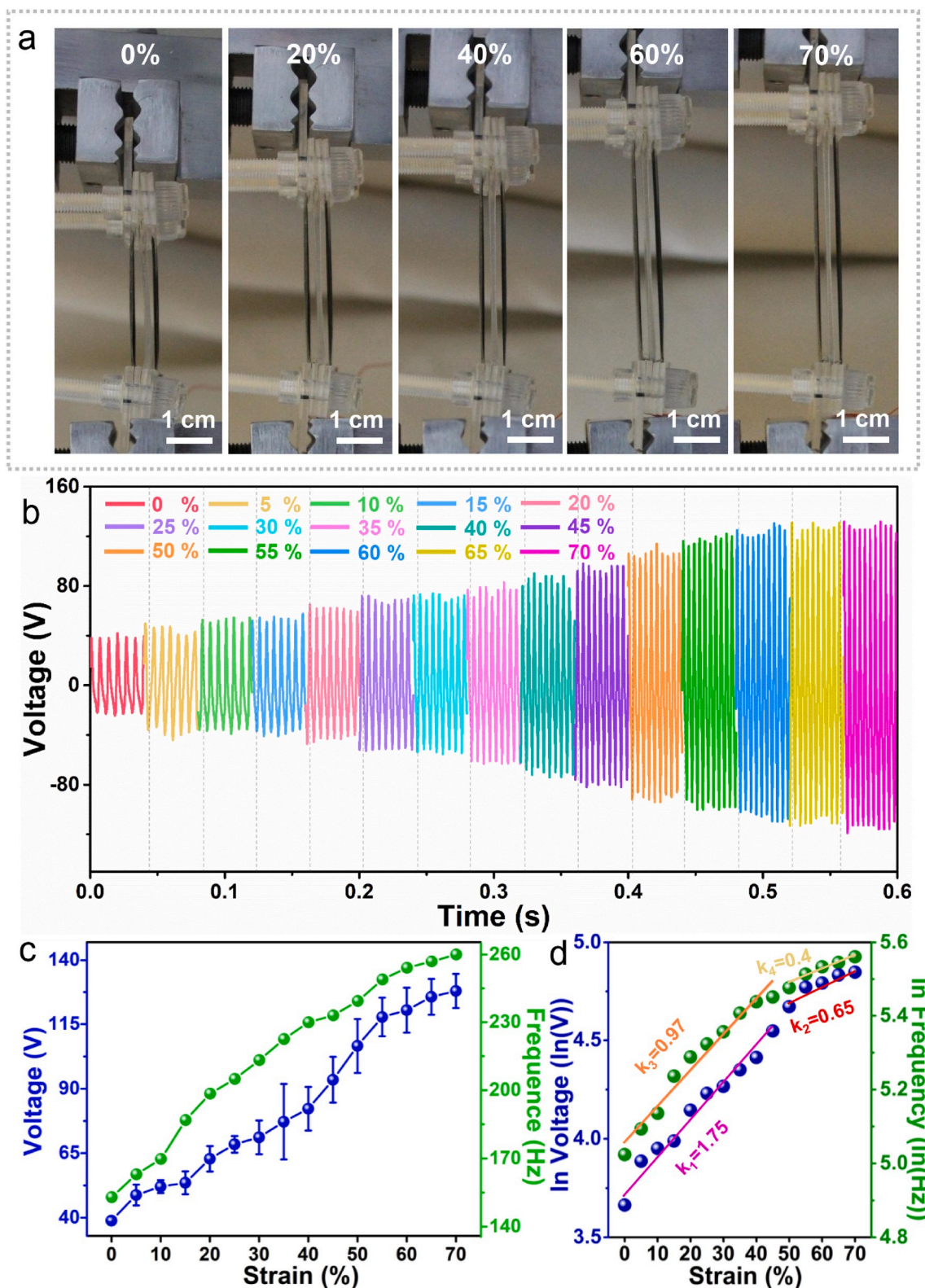


Fig. 5. The self-powered strain sensing performance of the TENG. (a) Photographs of the TENG in lateral view corresponding to different strains from 0% to 70%. (b) Dependence of the output voltage and vibration frequency of the TENG on stretchable strain. (c) Statistical results of experiment data in (b). (d) The linear fitting curves between the output voltage/vibration frequency and stretched strains.

#### 4. Conclusion

In summary, we have demonstrated a stretch-enhanced TENGs for efficient wind energy harvest and ultrasensitive strain sensing by using

stretchable PDMS-based graphene and PTFE composites, and the fabricated TENG exhibits excellent stretchability and working stability. Through improving device structure and applying stretched strain, the output performance of TENG can be greatly improved with large output

voltage and the output current of  $\sim 128$  V/7.2  $\mu$ A corresponding to the output power of 0.164 mW. The TENG can charge a 220  $\mu$ F capacitor to 1 V in 160 s as a power source, and it also presents a high strain sensitivity of 1.75 ln(V) at the strain from 0% to 45% as a stretchable strain sensor. This research illustrates the feasibility of utilizing stretchable TENG as a power source with a strain-tuned output power in smart city through harvesting natural wind energy. This stretchable TENG, fixed under the arch bridge, may exhibit huge application prospect in self-powered detecting deformation of the bridge, by harvesting the wind energy across the arch.

### Declaration of competing interest

The authors declare that they have no known competing financial interests or personal relationships that could have appeared to influence the work reported in this paper.

### CRediT authorship contribution statement

**Xue Zhao:** Formal analysis, Writing - original draft. **Ding Zhang:** Formal analysis, Writing - original draft. **Suwen Xu:** Data curation, Software. **Weiqi Qian:** Data curation, Validation. **Wei Han:** Formal analysis, Supervision. **Zhong Lin Wang:** Formal analysis, Supervision, Writing - review & editing. **Ya Yang:** Supervision, Conceptualization, Formal analysis, Writing - review & editing.

### Acknowledgments

X.Z. and D.Z. contributed equally to this work. Research was supported by the National Key R&D Program of China (Grant No. 2016YFA0202701), the National Natural Science Foundation of China (Grant Nos. 51472055), External Cooperation Program of BIC, Chinese Academy of Sciences (Grant No. 121411KYS820150028), the 2015 Annual Beijing Talents Fund (Grant No. 2015000021223ZK32), Qingdao National Laboratory for Marine Science and Technology (No. 2017ASKJ01), and the University of Chinese Academy of Sciences (Grant No. Y8540XX2D2).

### Appendix A. Supplementary data

Supplementary data to this article can be found online at <https://doi.org/10.1016/j.nanoen.2020.104920>.

### References

- [1] R. Giffinger, C. Fertner, H. Kramar, E. Meijers, Cent. Reg. Sci. Vienna (2007) 1–12.
- [2] S. Wang, X. Wang, Z.L. Wang, Y. Yang, ACS Nano 10 (2016) 5696–5700.
- [3] J.B. Goodenough, K. Park, J. Am. Chem. Soc. 135 (2013) 1167–1176.
- [4] Y. Zhu, S. Murali, M.D. Stoller, K.J. Ganesh, W. Cai, P.J. Ferreira, A. Pirkle, R. M. Wallace, K.A. Cychoz, M. Thommes, D. Su, E.A. Stach, R.S. Ruoff, Science 332 (2011) 1537–1541.
- [5] J.M. Tarascon, M. Armand, Nature 414 (2001) 359–367.
- [6] F.R. Fan, Z.Q. Tian, Z.L. Wang, Nano Energy 1 (2012) 328–334.
- [7] J. Chung, H. Yong, H. Moon, Q.V. Duong, S. Choi, D. Kim, Sangmin Lee, Adv. Sci. 5 (2018) 1801054.
- [8] C. Zhao, H. Feng, L. Zhang, Z. Li, Y. Zou, P. Tan, H. Ouyang, D. Jiang, M. Yu, C. Wang, H. Li, L. Xu, W. Wei, Z. Li, Adv. Funct. Mater. 29 (2019), 1808640.
- [9] K. Zhao, Y. Yang, X. Liu, Z.L. Wang, Adv. Energy Mater. 7 (2017), 1700103.
- [10] Y. Yang, G. Zhu, H. Zhang, J. Chen, X. Zhong, Z.-H. Lin, Y. Su, P. Bai, X. Wen, Z. L. Wang, ACS Nano 7 (2013) 9461–9468.
- [11] X. Zhao, B. Chen, G. Wei, J.M. Wu, W. Han, Y. Yang, Adv. Mater. Technol. 4 (2019), 1800723.
- [12] S. Wang, X. Mu, Y. Yang, C. Sun, A.Y. Gu, Z.L. Wang, Adv. Mater. 27 (2015) 240–248.
- [13] T. Quan, Y. Yang, Nano Res 9 (2016) 2226–2233.
- [14] J. Chen, Z.L. Wang, Joule 1 (2017) 480–521.
- [15] Y. Xi, J. Wang, Y. Zi, X. Li, C. Han, X. Cao, C. Hu, Z.L. Wang, Nano Energy 38 (2017) 101–108.
- [16] B.D. Chen, W. Tang, C. He, C.R. Deng, L.J. Yang, L.P. Zhu, J. Chen, J.J. Shao, L. Liu, Z.L. Wang, Mater. Today 21 (2018) 88–97.
- [17] Z.H. Lin, G. Cheng, S. Lee, K.C. Pradel, Z.L. Wang, Adv. Mater. 26 (2014) 4690–4696.

- [18] S.S. Kwak, S. Lin, J.H. Le, H. Ry, T.Y. Kim, H. Zhong, H. Chen, S.W. Kim, ACS Nano 10 (2016) 7297–7302.
- [19] B. Kim, J. Chung, H. Moon, D. Kim, S. Lee, Nano Energy 50 (2018) 133–139.
- [20] X. Chen, Y. Song, Z. Su, H. Chen, X. Cheng, J. Zhang, M. Han, H. Zhang, Nano Energy 38 (2017) 43–50.
- [21] K. Zhang, S. Wang, Y. Yang, Adv. Energy Mater. 7 (2017), 1601852.
- [22] X. Wang, Z.L. Wang, Y. Yang, Nano Energy 26 (2016) 164–171.
- [23] Y. Wu, Y. Yang, X. Wang, Z.L. Wang, Nano Energy 11 (2015) 162–170.
- [24] K. Zhang, Y. Yang, Nano Res 9 (2016) 974–984.
- [25] K. Zhang, Z.L. Wang, Y. Yang, ACS Nano 10 (2016) 9044–9052.
- [26] X. Chen, Y. Wu, J. Shao, T. Jiang, A. Yu, L. Xu, Z.L. Wang, Small 13 (2017), 1702929.
- [27] X. Pu, M. Liu, X. Chen, J. Sun, C. Du, Y. Zhang, J. Zhai, W. Hu, Z.L. Wang, Sci. Adv. 3 (2017), e1700015.
- [28] X. Pu, H. Guo, J. Chen, X. Wang, Y. Xi, C. Hu, Z.L. Wang, Sci. Adv. 3 (2017), e1700694.
- [29] M. Shi, H. Wu, J. Zhang, M. Han, B. Meng, H. Zhang, Nano Energy 3 (2017) 479–487.
- [30] D. Heo, T. Kim, H. Yong, K.T. Yoo, Sangmin Lee, Nano Energy 50 (2018) 1–8.
- [31] L. Xie, X. Chen, Z. Wen, Y. Yang, J. Shi, C. Chen, M. Peng, Y. Liu, X. Sun, Nano-Micro Lett. 11 (2019) 39.
- [32] M. Peng, Z. Wen, L. Xie, J. Cheng, Z. Jia, D. Shi, H. Zeng, B. Zhao, Z. Liang, T. Li, L. Jiang, Adv. Mater. 31 (2019), 1902930.
- [33] Z. Wen, Y. Yang, N. Sun, G. Li, Y. Liu, C. Chen, J. Shi, L. Xie, H. Jiang, D. Bao, Q. Zhuo, X. Sun, Adv. Funct. Mater. 28 (2018), 1803684.
- [34] K.S. Novoselov, A.K. Geim, S.V. Morozov, D. Jiang, Y. Zhang, S.V. Dubonos, I. V. Grigorieva, A.A. Firsov, Science 306 (2004) 666.
- [35] A.K. Geim, K.S. Novoselov, Nat. Mater. 6 (2007) 183.
- [36] A.A. Balandin, S. Ghosh, W. Bao, I. Calizo, D. Teweldebrhan, F. Miao, C.N. Lau, Nano Lett. 8 (2008) 902–907.
- [37] C. Yan, J. Wang, W. Kang, M. Cui, X. Wang, C.Y. Foo, K.J. Chee, P.S. Lee, Adv. Mater. 26 (2014) 2022–2027.
- [38] Z. Wang, W. Gao, Q. Zhang, K. Zheng, J. Xu, W. Xu, E. Shang, J. Jiang, J. Zhang, Y. Liu, ACS Appl. Mater. Interfaces 11 (2018) 1344–1352.
- [39] D. Zhang, Y. Song, L. Ping, S. Xu, D. Yang, Y. Wang, Y. Yang, Nano Res 12 (2019) 2982–2987.
- [40] Y. Liu, W. Hao, H. Yao, S. Li, Y. Wu, J. Zhu, L. Jiang, Adv. Mater. 30 (2018), 1705377.
- [41] D. Zhang, K. Zhang, Y. Wang, Y. Wang, Y. Yang, Nano Energy 56 (2019) 25–32.
- [42] S.A. Shankaregowda, R.F.S.M. Ahmed, C.B. Nanjagowda, J. Wang, S. Guana, M. Puttaswamy, A. Amini, Y. Zhang, D. Kong, K. Sannathammegowda, F. Wang, C. Cheng, Nano Energy 66 (2019), 104141.
- [43] M.K. Kim, M.S. Kim, H.B. Kwon, S.E. Jo, Y.J. Kim, RSC Adv. 7 (2017) 48368–48373.
- [44] N. Lu, C. Lu, S. Yang, J. A. Rogers, Adv. Funct. Mater. 22 (2012) 4044.
- [45] Q. Liu, J. Chen, Y. Li, G. Shi, ACS Nano 10 (2016) 7901–7906.
- [46] J. Chung, H. Yong, H. Moon, S.T. Choi, D. Bhatia, D. Choi, D. Kim, S. Lee, Adv. Energy Mater. 8 (2018) 1703024.
- [47] J. Chung, D. Heo, G. Shin, D. Choi, K. Choi, D. Kim, S. Lee, Adv. Energy Mater. 9 (2018), 1901731.



**Xue Zhao** is a Ph.D student at Key Laboratory of Physics and Technology for Advanced Batteries (Ministry of Education), Jilin University. She is a visiting student and pursuing her doctoral degree in research group of Prof. Ya Yang at Beijing Institute of Nanoenergy and Nanosystems, Chinese Academy of Sciences (CAS). She received her B.S. from Jilin University in 2016. Her research interests focus on harvesting mechanical energy, preparation of triboelectric nanogenerator and self-powered sensors based triboelectric nanogenerator.



**Ding Zhang** is a Ph.D. student in the research group of Prof. Ya Yang at Beijing Institute of Nanoenergy and Nanosystems, CAS. He received his master's degree (2017) in Materials Science from Lanzhou Institute of Chemical Physics, CAS. He received his bachelor's degree (2014) in Materials Science and Engineering from China University of Mining and Technology. His research interests focus on flexible electronic devices and self-powered sensing systems.



**Suwen Xu** is a Ph.D student at Minzu University of China. She is currently a visiting student in the research group of Prof. Ya Yang at Beijing Institute of Nanoenergy and Nanosystems, Chinese Academy of Sciences (CAS). Her research interests focus on nanostructured materials for photo/piezocatalysis and their coupling effect.



**Weiqi Qian** is currently a student in the research group of Prof. Ya Yang at Beijing Institute of Nanoenergy and Nanosystems, Chinese Academy of Sciences (CAS). Her recent research interests are ferroelectric and piezoelectric materials for electrochemical applications.



**Prof. Wei Han** is a Professor at College of Physics, Jilin University. He is also the Executive Deputy Director of the International Center of Future Science, Jilin University. He received his Ph.D. in Solid-State Physics from Tomsk Polytechnic University in 1997. He works on the application of supercapacitor in the fields of electric vehicles and new energy resource (solar and wind energy), design of electrode materials for producing hydrogen by electrolysed water, and application of nanomaterials in the field of nuclear wastewater purification. He has published more than 50 journal papers, and obtained more than 20 patents.



**Prof. Zhong Lin (ZL) Wang** received his Ph.D. from Arizona State University in physics. He now is the Hightower Chair in Materials Science and Engineering, Regents' Professor, Engineering Distinguished Professor and Director, Center for Nanostructure Characterization, at Georgia Tech. Dr. Wang has made original and innovative contributions to the synthesis, discovery, characterization and understanding of fundamental physical properties of oxide nanobelts and nanowires, as well as applications of nanowires in energy sciences, electronics, optoelectronics and biological science. His discovery and breakthroughs in developing nanogenerators established the principle and technological road map for harvesting mechanical energy from environment and biological systems for powering personal electronics. His research on self-powered nanosystems has inspired the worldwide effort in academia and industry for studying energy for micro-nano-systems, which is now a distinct disciplinary in energy research and future sensor networks. He coined and pioneered the field of piezotronics and piezophotonics by introducing piezoelectric potential gated charge transport process in fabricating new electronic and optoelectronic devices. Details can be found at: <http://www.nanoscience.gatech.edu>.



**Prof. Ya Yang** received his Ph.D. in Materials Science and Engineering from University of Science and Technology Beijing, China. He is currently a professor at Beijing Institute of Nanoenergy and Nanosystems, Chinese Academy of Sciences, China. He has developed various new hybridized and multi-effects coupled nanogenerators, opening up the new principles of the device design and coupled effects, and the new approaches of improving output performances of energy-related devices. His main research interests focus on the field of hybridized and coupled nanogenerators for energy conversion, self-powered sensing, and some new physical effects. Details can be found at: <http://www.researcherid.com/rid/A-7219-2016>.